Metal−Porphyrinogen Organometallic Chemistry: The Intramolecular Reactivity of η^2-Acyls Bonded to Titanium(IV)−*meso*-Octaethyl Mono(pyridine)−Tris(pyrrole) and to Vanadium(III)−*meso*-Octaethyl Bis(pyridine)−Bis(pyrrole) Macrocycle

Raffaella Crescenzi, Euro Solari, and Carlo Floriani*

Institut de Chimie Minérale et Analytique, BCH, Université de Lausanne, CH-1015 Lausanne, Switzerland

Nazzareno Re

Facoltà di Farmacia, Università degli Studi "G. D'Annunzio", I-66013 Chieti, Italy

Angiola Chiesi-Villa and Corrado Rizzoli

Dipartimento di Chimica, Università di Parma, I-43100 Parma, Italy

Received October 29, 1998

The organometallic chemistry of titanium− and vanadium−macrocycle was investigated using *meso*-octaethyl mono(pyridine)−tris(pyrrole), $[Et_8(C_5H_3N)(C_4H_2NH)_3]$, **1**, and *meso*-octaethyl *cis*-bis(pyridine)−bis(pyrrole), $[Et_8$*cis*-$(m\text{-}MeC_5H_2N)(C_5H_3N)(C_4H_2NH)_2]$, **7**, as ligands for titanium(IV) and vanadium(III), respectively. The metalation of **1** with LiBu followed by the reaction with $TiCl_4{\cdot}thf_2$ led to $[Et_8(C_5H_3N)(C_4H_2N)_3Ti{-}Cl]$, **3**, which was alkylated to $[Et_8(C_5H_3N)(C_4H_2N)_3Ti{-}Me]$, **4**. The Ti−C bond in **4** underwent a migratory insertion reaction with Bu^tNC and carbon monoxide. In the former case the corresponding η^2-iminoacyl was isolated and structurally characterized as $[Et_8(C_5H_3N)(C_4H_2N)_3Ti(\eta^2\text{-}C(Me)NBu^t)]$, **6**, while the reaction of **4** with carbon monoxide led to the homologation of one pyrrolyl anion, thus converting the mono(pyridine)−tris(pyrrole) into a *cis*-bis(pyridine)−bis(pyrrole) macrocycle and the oxotitanium(IV) functionality in $[Et_8(m\text{-}MeC_5H_2N)(C_5H_3N)(C_4H_2N)_2Ti{=}O]$, **5**. The homologation occurs via a carbenium ion η^2-acyl which was not intercepted. The synthesis of $[Et_8(m\text{-}MeC_5H_2N)(C_5H_3N)(C_4H_2N)_2V{-}Cl]$, **9**, was carried out from the lithiated form, **8**, of **7** followed by reaction with $VCl_3{\cdot}thf_3$. Complex **9** was converted into the corresponding methyl derivative $[Et_8(m\text{-}MeC_5H_2N)(C_5H_3N)(C_4H_2N)_2V{-}Me]$, **10**, which underwent a migratory insertion of CO and Bu^tNC. The reaction of **10** with Bu^tNC led to the expected η^2-iminoacyl $[Et_8(m\text{-}MeC_5H_2N)(C_5H_3N)(C_4H_2N)_2V\{\eta^2\text{-}C(Me){=}NBu^t\}]$, **12**, while in the case of CO, the intermediate η^2-acyl, behaving as a nucleophilic carbenoid, reacted preferentially with the pyridine α-position, leading to $[Et_8(m\text{-}MeC_5H_3N)\mu(O{-}CMe)(C_4H_2N)\}(C_4H_2N)\text{-}(C_5H_3N)V]$, **11**. The proposed structures were supported by the X-ray analysis of **5**, **6**, **8**, **9**, and **11**.

Introduction

The organometallic chemistry developed inside a cavity can produce very reactive intermediates, which can display unprecedented reactivity as a result of unavailable intermolecular pathways. Such a protecting metal environment can be provided by an appropriate macrocyclic ligand,[1−4] which should, however, contain at the same time reactive sites that act as a target for the organometallic functionality generated in the cavity. The macrocycle-based organometallic chemistry mentioned above has been greatly developed using the *meso*-octaethylporphyrinogen tetraanion,[5] **A**, and led us to discover (i) the homologation of a macrocyclic ligand using carbon monoxide;[6] (ii) the intramolecular and intermolecular aliphatic C−H activation;[7] and (iii) the bifunctional carrying properties of polar organometallics.[5c,8] The *meso*-octaethyl mono(pyridine) tris(pyrrole), **B**, and *meso*-octaethyl bis(pyridine) bis(pyrrole), **C**, (Chart 1), which have no precedent in organometallic and coordination chemistry (except for a single example in the case of hafnium),[6b] may serve as particularly interesting ancillary ligands in early-transition-metal chemistry. Ligands **B** and **C** maintain the conformational peculiarities of the *meso*-octaalkylporphyrinogen[5−8] and are very different as a result of the following: (i)

* To whom correspondence should be addressed.

(1) For leading references on organometallic chemistry based on macrocyclic ligands see refs 2−4.

10.1021/om980888o CCC: $18.00
Publication on Web 01/26/1999

Chart 1

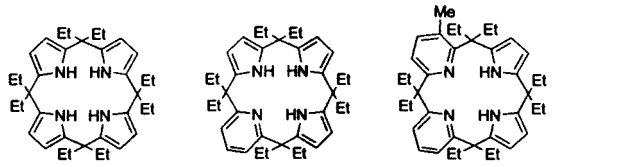

the change in the overall charge allows one to work with neutral rather than bimetallic or ion pair complexes; (ii) replacing a pyrrole with a pyridine modifies not only the electronic properties of the ligand but also the size of the cavity, with the pyridine ring becoming a spectator ligand able to protect a coordinatively unsaturated metal. Preliminary results have been communicated.[9]

We report here the use of macrocycles **B** and **C**, derived from the mono- and bis-homologation of **A**, as ancillary ligands for titanium(IV) and vanadium(III), respectively, with the purpose of studying their organometallic functionalization. The very reactive η^2-acyls (carbenium ion) formed at the metal reacted intramolecularly with the resulting homologation of the pyrrole ring in the case of titanium, while in the case of vanadium the nucleophilic properties of the acyl group led to attack on the pyridine ring. In the former case, the complete cleavage of the C−O bond was followed by the formation of oxo-metal species. An extended Hückel calculation section deals in general with the homologation reaction and with the change in the reactivity of the intermediate η^2-acyl from electrophilic to nucleophilic character, depending on the nature of the metal.

Experimental Section

General Procedure. All reactions were carried out under an atmosphere of purified nitrogen. Solvents were dried and distilled before use by standard methods. ^{1}H NMR and IR spectra were recorded on AC-200, DPX-400 Bruker, and Perkin-Elmer FT 1600 instruments, respectively. GC and GC−MS analyses were carried out using a HP 5890 Series II system and an HP 5890A GC system, respectively. The syntheses of **1**, **2**, **7**, and **8** were carried out as reported in ref 6b.

Synthesis of 3. $TiCl_4$·thf_2 (2.25 g, 6.7 mmol) and **2** were added to benzene (200 mL). The resulting dark red solution was stirred at room temperature for 1 day. The violet solid that formed was extracted with the mother liquor to eliminate LiCl. The solution was evaporated to dryness and the violet solid triturated with pentane (150 mL), filtered, and dried (3.28 g, 79%). Anal. Calcd for $C_{37}H_{49}ClN_4Ti$: C, 70.19; H, 7.80; N, 8.85. Found: C, 70.31; H, 7.94; N, 8.50. ^{1}H NMR (CD_2Cl_2; 25 °C): δ 7.77 (t, C_5H_3N, 1H, J = 7.8 Hz), 7.26 (d, C_5H_3N, 2H, J = 7.8 Hz), 6.02 (d, C_4H_2N, 2H), 5.89 (d, C_4H_2N, 4H), 2.57 (m, CH_2, 2H), 2.34−2.04 (m, CH_2, 10H), 1.83−1.68 (m, CH_2, 4H), 0.95 (t, CH_3, 6H), 0.74 (q, CH_3, 12H), 0.53 (t, CH_3, 6H).

Synthesis of 4. MeLi (4 mL, 2M in Et_2O, 2.8 mmol) was added dropwise to a melting violet suspension of **3** (1.36 g, 2.2 mmol) in frozen benzene (200 mL). The resulting dark red solution was stirred for 3 h at room temperature after the conclusion of the addition. The solvent was evaporated, and to the remaining brown solid was added Et_2O (200 mL). The undissolved white solid, LiCl, was removed by filtration. After evaporation the solid was triturated with pentane (100 mL) and a dark red solid was filtered off and dried in vacuo (1.1 g, 77%). Anal. Calcd for $C_{38}H_{52}N_4Ti$: C, 74.49; H, 8.55; N, 9.14. Found: C, 74.26; H, 8.43; N, 8.81. ^{1}HNMR (C_6D_6, 25 °C): δ 7.08 (t, C_5H_3N, 1H, J = 7.8 Hz), 6.78 (d, C_5H_3N, 2H, J = 7.8 Hz), 6.16 (s, C_4H_2N, 2H), 5.76 (bs, C_4H_2N, 1H), 5.74 (bs, C_4H_2N, 1H), 5.17 (bs, C_4H_2N, 1H), 5.16 (bs, C_4H_2N, 1H), 2.81−1.92 (m, CH_2, 14H), 1.55 (m, CH_2, 2H), 1.28 (s, CH_3−Ti, 3H), 1.12 (s, CH_3, 6H), 0.93 (t, CH_3, 6H), 0.66 (m, CH_3, 12H).

Synthesis of 5. A red solution of **4** (1.43 g, 2.3 mmol) in benzene (150 mL) was exposed to CO (1 atm) for 4−5 days at room temperature. An orange microcrystalline solid formed. The solvent was evaporated, and the red-orange solid was triturated with *n*-hexane (100 mL), filtered, and dried in vacuo (70%). Recrystallization of the powder from benzene/*n*-hexane at room temperature gave orange crystals containing benzene

(2) For tmtaa [dibenzotetramethyltetraaza[14]annulene], see: (a) Goedken, V. L.; Ladd, J. A. *J. Chem. Soc., Chem. Commun.* **1981**, 910; **1982**, 142. (b) Floriani, C.; Ciurli, S.; Chiesi-Villa, A.; Guastini, C. *Angew. Chem., Int. Ed. Engl.* **1987**, *26*, 70. (c) Solari, E.; De Angelis, S.; Floriani, C.; Chiesi-Villa, A.; Rizzoli, C. *Inorg. Chem.* **1992**, *31*, 96. (d) De Angelis, S.; Solari, E.; Gallo, E.; Floriani, C.; Chiesi-Villa, A.; Rizzoli, C. *Inorg. Chem.* **1992**, *31*, 2520. (e) Giannini, L.; Solari, E.; Floriani, C.; Chiesi-Villa, A.; Rizzoli, C. *Angew. Chem., Int. Ed. Engl.* **1994**, *33*, 2204. (f) Giannini, L.; Solari, E.; De Angelis, S.; Ward, T. R.; Floriani, C.; Chiesi-Villa, A.; Rizzoli, C. *J. Am. Chem. Soc.* **1995**, *117*, 5801. (g) Black, D. G.; Swenson, D. C.; Jordan, R. F. *Organometallics* **1995**, *14*, 3539. (h) Blake, A. J.; Mountford, P.; Nikonov, G. I.; Swallow, D. *Chem. Commun.* **1996**, 1835. (i) Schumann, H. *Inorg. Chem.* **1996**, *35*, 1808. (j) Nikonov, G. I.; Blake, A. J.; Mountford, P. *Inorg. Chem.* **1997**, *36*, 1107. (k) Black, D. G.; Jordan, R. F.; Rogers, R. D. *Inorg. Chem.* **1997**, *36*, 103. (l) Martin, A.; Uhrhammer, R.; Gardner, T. G.; Jordan, R. F. *Organometallics* **1998**, *17*, 382. (m) Mountford, P. *Chem. Soc. Rev.* **1998**, *27*, 105.

(3) For porphyrins, see: (a) Brand, H.; Arnold, J. *Angew. Chem., Int. Ed. Engl.* **1994**, *33*, 95. (b) Brand, H.; Arnold, J. *Organometallics* **1993**, *12*, 3655. (c) Kim, H.-J.; Whang, D.; Kim K.; Do, Y. *Inorg. Chem.* **1993**, *32*, 360. (d) Arnold, J.; Johnson, S. E.; Knobler C. B.; Hawthorne, M. F. *J. Am. Chem. Soc.* **1992**, *114*, 3996. (e) Brand H.; Arnold, J. *J. Am. Chem. Soc.* **1992**, *114*, 2266. (f) Brand H.; Arnold, J. *Coord. Chem. Rev.* **1995**, *140*, 137. (g) Aida T.; Inoue, S. *Acc. Chem. Res.* **1996**, *29*, 39. (h) Collman, J. P.; Barnes, C. E.; Swepston, P. N.; Ibers, J. A. *J. Am. Chem. Soc.* **1984**, *106*, 3500. (i) Collman, J. P.; Brothers, P. J.; Mc-Elwee-White, L.; Rose, E.; Wright, L. J. *J. Am. Chem. Soc.* **1985**, *107*, 4570. (j) Collman, J. P.; Brothers, P. J.; McElwee-White, L.; Rose, E. *J. Am. Chem. Soc.* **1985**, *107*, 6110.

(4) For calix[4]arenes, see: (a) Giannini, L.; Solari, E.; Zanotti-Gerosa, A.; Floriani, C.; Chiesi-Villa, A.; Rizzoli, C. *Angew. Chem., Int. Ed. Engl.* **1996**, *35*, 85 and 2825; **1997**, *36*, 753. (b) Castellano, B.; Zanotti-Gerosa, A.; Solari, E.; Floriani, C.; Chiesi-Villa, A.; Rizzoli, C. *Organometallics* **1996**, *15*, 4894. (c) Giannini, L.; Caselli, A.; Solari, E.; Floriani, C.; Chiesi-Villa, A.; Rizzoli, C.; Re, N.; Sgamellotti, A. *J. Am. Chem. Soc.* **1997**, *119*, 9198 and 9709. (d) Caselli, A.; Giannini, L.; Solari, E.; Floriani, C.; Re, N.; Chiesi-Villa, A.; Rizzoli, C. *Organometallics* **1997**, *16*, 5457. (e) Zanotti-Gerosa, A.; Solari, E.; Giannini, L.; Floriani, C.; Chiesi-Villa, A.; Rizzoli, C. *J. Am. Chem. Soc.* **1998**, *120*, 437. (f) Giannini, L.; Solari, E.; Floriani, C.; Chiesi-Villa, A.; Rizzoli, C. *J. Am. Chem. Soc.* **1998**, *120*, 823.

(5) (a) De Angelis, S.; Solari, E.; Floriani, C.; Chiesi-Villa, A.; Rizzoli, C. *J. Chem. Soc., Dalton Trans.* **1994**, 2467, and references therein. (b) Jacoby, D.; Floriani, C.; Chiesi-Villa, A.; Rizzoli, C. *J. Chem. Soc., Chem. Commun.* **1991**, 790. (c) Jacoby, D.; Floriani, C.; Chiesi-Villa, A.; Rizzoli, C. *J. Am. Chem. Soc.* **1993**, *115*, 3595. (d) Solari, E.; Musso, F.; Floriani, C.; Chiesi-Villa, A.; Rizzoli, C. *J. Chem. Soc., Dalton Trans.* **1994**, 2015.

(6) (a) Jacoby, D.; Floriani, C.; Chiesi-Villa, A.; Rizzoli, C. *J. Am. Chem. Soc.* **1993**, *115*, 7025. (b) Jacoby, D.; Isoz, S.; Floriani, C.; Chiesi-Villa, A.; Rizzoli, C. *J. Am. Chem. Soc.* **1995**, *117*, 2793. (c) Floriani, C. In *Stereoselective Reactions of Metal-Activated Molecules*; Werner, H., Sundermeyer, J., Eds.; Vieweg: Wiesbaden, Germany, 1995; pp 97−106.

(7) (a) Floriani, C. *Pure Appl. Chem.* **1996**, *68*, 1. (b) Jacoby, D.; Isoz, S.; Floriani, C.; Chiesi-Villa, A.; Rizzoli, C. *J. Am. Chem. Soc.* **1995**, *117*, 2805. (c) Isoz, S.; Floriani, C.; Schenk, K.; Chiesi-Villa, A.; Rizzoli, C. *Organometallics* **1996**, *15*, 337. (d) Kretz, C. M.; Gallo, E.; Solari, E.; Floriani, C.; Chiesi-Villa, A.; Rizzoli, C. *J. Am. Chem. Soc.* **1994**, *116*, 10775. (e) De Angelis, S.; Solari, E.; Floriani, C.; Chiesi-Villa, A.; Rizzoli, C. *Angew. Chem., Int. Ed. Engl.* **1995**, *34*, 1092.

(8) (a) De Angelis, S.; Solari, E.; Floriani, C.; Chiesi-Villa, A.; Rizzoli, C. *Organometallics* **1995**, *14*, 4505. (b) Jacoby, D.; Isoz, S.; Floriani, C.; Schenk, K.; Chiesi-Villa, A.; Rizzoli, C. *Organometallics* **1995**, *14*, 4816. (c) Solari, G.; Solari, E.; Floriani, C.; Chiesi-Villa, A.; Rizzoli, C. *Organometallics* **1997**, *16*, 508.

(9) (a) Crescenzi, R.; Solari, E.; Floriani, C.; Chiesi-Villa, A.; Rizzoli, C. *Organometallics* **1996**, *15*, 5456. (b) Solari, E.; Crescenzi, R.; Jacoby, D.; Floriani, C.; Chiesi-Villa, A.; Rizzoli, C. *Organometallics* **1996**, *15*, 2685.

Table 1. Experimental Data for the X-ray Diffraction Studies on Crystalline Complexes 5, 6, 8, 9, and 11

complex	**5**	**6**	**8**	**9**	**11**
formula	$C_{39}H_{52}N_4OTi \cdot C_6H_6$	$C_{43}H_{61}N_5Ti$	$C_{43}H_{60}Li_2N_4O$	$C_{39}H_{52}ClN_4V \cdot 0.5C_7H_8$	$C_{41}H_{55}N_4OV \cdot 0.35C_6H_{14} \cdot 0.3C_4H_8O$
a, Å	11.990(2)	18.975(5)	11.689(2)	21.601(2)	11.700(4)
b, Å	17.186(3)	20.568(5)	19.153(3)	11.063(1)	17.698(6)
c, Å	11.559(2)	10.979(3)	10.152(2)	33.028(3)	18.557(9)
α, deg	101.79(2)	90.93(2)	100.86(2)	90	90
β, deg	117.78(2)	93.41(2)	113.73(2)	97.16(2)	92.56(6)
γ, deg	97.83(1)	112.92(2)	72.20(2)	90	90
V, Å^3	1987.8(8)	3936.0(19)	1975.5(7)	7831.2(13)	3839(3)
Z	2	4	2	8	4
fw	718.9	695.9	662.9	709.3	722.7
space group	$P\bar{1}$	$P\bar{1}$	$P\bar{1}$	$C2/c$	$P2_1/n$
T, °C	22	22	22	22	−130
λ, Å	1.541 78	1.541 78	1.541 78	1.541 78	1.541 78
ρ_{calc}, g cm^{-3}	1.201	1.174	1.114	1.203	1.250
μ, cm^{-1}	21.01	20.92	4.68	30.17	24.64
transmission coeff	0.665−1.000	0.715−1.000	0.992−1.000	0.443−1.000	0.768−1.000
R[a]	0.049	0.066	0.080	0.077	0.079
wR2[b]	0.147	0.207	0.284	0.276	0.234

[a] $R = \sum|\Delta F|/\sum|F_o|$ calculated on the unique observed data [$I > 2\sigma(I)$]. [b] $wR2 = [\sum w|\Delta F^2|^2/\sum w|F_o^2|^2]^{1/2}$ calculated on the unique total data with $I > 0$.

of crystallization and suitable for X-ray analysis. Anal. Calcd for **5**, $C_{39}H_{52}N_4OTi$: C, 73.11; H, 8.18; N, 8.74. Found: C, 73.49; H, 8.05; N, 8.54. ^{1}HNMR (CD_2Cl_2, 25 °C): δ 8.01 (t, C_5H_3N, 1H, J = 7.9 Hz), 7.71 (d, C_5H_3N, 1H, J = 7.9 Hz), 7.56 (d, C_5H_3N, 1H, J = 7.8 Hz), 7.51 (s, C_6H_5N, 2H), 6.08 (m, C_4H_2N, 2H,) 5.96 (m, C_4H_2N, 2H), 3.18 (m, CH_2, 2H), 2.73−2.39 (m, CH_2, 4H), overlapping with 2.51 (s, CH_3−pyridine, 3H), 2.14−1.86 (m, CH_2, 8H), 1.34 (m, CH_2, 2H), 0.89−0.55 (m, CH_3, 21H), 0.54 (t, CH_3, 3H). IR (Nujol): 1610 (s), 1077 (s), 968 (s), 747 (s), 686 (s) cm^{-1}.

Synthesis of 6. A benzene solution (30 mL) of Bu^{t}NC (0.3 mL, 2.7 mmol) was added dropwise to a dark red solution of **4** (1.65 g, 2.7 mmol) in benzene (150 mL). The mixture was stirred for 1 day, and the solvent of the resulting dark green solution was removed under reduced pressure. The residue was triturated with *n*-hexane (100 mL), and the dark green solid was filtered and dried in vacuo (1.4 g, 74%). Crystals suitable for X-ray analysis were obtained from the recrystallization of the powder in benzene/*n*-hexane at room temperature. Anal. Calcd for $C_{43}H_{61}N_5Ti$: C, 74.22; H, 8.84; N, 10.06. Found: C, 73.96, H, 8.75; N, 9.85. ^{1}HNMR (C_6D_6, 25 °C): δ 7.16 (t, C_5H_3N, 1H), 6.95 (d, C_5H_3N, 1H), 6.86 (d, C_5H_3N, 2H), 6.57 (d, C_5H_3N, 1H), 6.55 (s, C_4H_2N, 2H), 6.36 (q, C_4H_2N, 2H), 3.27 (m, thf, 4H), 2.45 (m, CH_2, 2H), 2.09 (s, CH_3−pyr, 3H), 1.94−2.21 (m, CH_2, 14H), 1.20 (m, thf, 4H), 0.99 (t, CH_3, 6H), 0.90 (t, CH_3, 6H), 0.73 (t, CH_3, 6H), 0.56 (t, CH_3, 6H).

Synthesis of 8. Bu^{n}Li (20.6 mL, 33.0 mmol) was added dropwise to a thf (100 mL) solution of Py_2Pyr_2 (9.50 g, 16.5 mmol), and then the solution was heated at 60 °C for 1 h and evaporated to dryness. The resulting oily residue was dissolved in *n*-hexane (100 mL). Upon complete evaporation the *n*-hexane solution gave a beige powder, which was collected using 50 mL of *n*-hexane (85%). Anal. Calcd for $[Et_8N_2N_2Li_2(thf)_2]$, $C_{47}H_{68}N_4O_2Li_2$: C, 76.83; H, 9.26; N, 7.63. Found: C, 76.43, H, 9.01; N, 7.49. ^{1}HNMR (C_6D_6): δ 7.02 (t, C_5H_3N, 1H, J = 7.8 Hz), 6.79 (d, C_5H_3N, 2H, J = 7.8 Hz), 6.40 (s, C_4H_2N, 2H), 6.21−6.17 (m, C_4H_2N, 4H), 2.39−1.76 (m, CH_2, 10H), overlapping with 1.88 (s, Me, 3H), 1.42−0.77 (m, CH_2 and CH_3, 16H), 0.69−0.40 (m, CH_3, 14H), overlapping with 0.45 (s, Bu^t, 9H). IR (Nujol; C═N): 1655 (vs) cm^{-1}. The powder recrystallized from warm *n*-hexane gave white crystals suitable for X-ray analysis, and they contain a single thf molecule.

Synthesis of 9. $VCl_3 \cdot thf_3$ (9.90 g, 26.50 mmol) was added to a suspension of **8** (17.5 g, 26.4 mmol) in toluene (500 mL). The suspension was stirred overnight at room temperature to give a deep brown solution and solid precipitate, which was removed by filtration. The resulting solution was evaporated to dryness. The solid collected with *n*-hexane (400 mL) gave a microcrystalline solid. Toluene was then added until the solid had almost completely dissolved, and the undissolved solid was filtered out. The solution was evaporated to dryness and the solid collected with *n*-hexane (200 mL) (75%). The solid was recrystallized at room temperature from toluene/*n*-hexane and gave deep yellow crystals for the X-ray analysis. Anal. Calcd for **9**·thf, $C_{43}H_{60}ClN_4OV$: C, 70.23; H, 8.22; N, 7.62. Found: C, 70.82; H, 8.27; N, 7.79. μ_{eff} = 2.93 μ_B at 297 K.

Synthesis of 10. MeLi (10.0 mol) was added dropwise at room temperature to a suspension of **9** (7.26 g, 9.87 mmol) in *n*-hexane. During this process the suspension became deep red. The solvent was evaporated to dryness, and the solid, recrystallized at room temperature from a mixture of toluene/*n*-hexane, gave red crystals of **10** (51.0%). The low yield is due to rather high solubility in *n*-hexane. Anal. Calcd for **10**, $C_{40}H_{55}N_4V$ (MW 642): C, 74.76; H, 8.57; N, 8.72. Found: C, 74.54; H, 9.05, N, 8.67. μ_{eff} = 2.79 μ_B at 295 K.

Synthesis of 11. A thf (30 mL) solution of **10** (1.60 g) was kept under carbon monoxide for 1 h at room temperature. The red solution turned deep brown. The thf was evaporated to dryness and the residue, collected with *n*-hexane, crystallized (82%). Crystals suitable for the X-ray analysis were obtained from thf/*n*-hexane at room temperature. Anal. Calcd for $C_{41}H_{55}N_4OV$: C, 73.43; H, 8.21, N, 8.36. Found: C, 73.56; H, 8.27; N, 8.00. μ_{eff} = 3.12 μ_B at 297 K.

Synthesis of 12. To a benzene (80 mL) solution of **10** (3.9 g, 6.1 mmol) was added Bu^{t}NC (0.51 g, 6.1 mmol). The solution became pale in color, while the product slowly formed. The suspension was kept at room temperature for 12 h, then the solvent was evaporated to dryness and the green solid collected with *n*-hexane (75 mL), filtered, and dried (3.4 g, 77%). Anal. Calcd for $C_{45}H_{64}N_5V$: C, 74.45; H, 8.89; N, 9.65. Found: C, 74.44; H, 8.55; N, 9.66. IR (Nujol, ν_{max}/cm^{-1}): 3077 (w), 1648 (s), 1588 (s), 1567 (s), 11305 (m), 1239 (s), 1188 (m), 1072 (s), 739 (s), 678 (s). μ_{eff} = 2.55 μ_B a 295 K.

X-ray Crystallography for Complexes 5, 6, 8, 9, and 11. Suitable crystals were mounted in glass capillaries and sealed under nitrogen. The reduced cells were obtained with the use of TRACER.[10] Crystal data and details associated with data collection are given in Table 1 and Table S1. Data were collected on a single-crystal diffractometer (Rigaku AFC6S) at 295 K for **5**, **6**, **8**, **9** and 133 K for **11**. For intensities and background the individual reflection profiles were analyzed.[11] The structure amplitudes were obtained after the usual Lorentz and polarization[12] corrections, and the absolute scale was established by the Wilson method.[13] The crystal quality was tested by ψ scans showing that crystal absorption effects could be neglected only for **8**. For the other complexes data

were corrected for absorption using ABSORB[14] for **5** and **9** and a semiempirical method[15] for **6** and **11**. The function minimized during the full-matrix least-squares refinements was $\sum w(\Delta F^2)^2$. Anomalous scattering corrections were included in all structure factor calculations.[16b] Scattering factors for neutral atoms were taken from ref 16a for nonhydrogen atoms and from ref 17 for H. Structure solutions were based on the observed reflections [$I > 2\sigma(I)$], while the refinements were based on the unique reflections having $I > 0$. The structures of **5**, **6**, **9**, and **11** were solved by the heavy-atom method starting from a three-dimensional Patterson map.[18] The structure of **8** was solved by direct methods using SHELX86.[19] Refinements were done by full-matrix least-squares, first isotropically and then anisotropically for all non-H atoms except for the disordered atoms in **8**, **9**, and **11**. The hydrogen atoms were located in a difference Fourier map (**5**, **9**, and **11**) or put in geometrically calculated positions (**6** and **8**) and introduced in the refinements as fixed atom contributions ($U_{iso} = 0.05$ Å^2 for **11**, 0.08 Å^2 for **5**, 0.10 Å^2 for **6**, and 0.12 Å^2 for **8** and **9**). The H atoms associated with the disordered carbon atoms were ignored. In the last stage of refinement the weighting scheme $w = 1/[\sigma^2(F_o^2) + (aP)^2]$ (with $P = (F_o^2 + 2F_c^2)/3$ was applied with a resulting in the values of 0.0915, 0.0891, 0.1763, 0.1788, and 0.1520 for **5**, **6**, **8**, **9**, and **11**, respectively. All calculations were performed by using SHELX92.[20] The final difference map for **6**, **8**, and **9** showed no unusual features, with no significant peaks above the general background. For complex **5** two residual peaks of 0.87 and 0.68 e Å^{-3} were found in the near proximity of the metal atom in the direction of the Ti−N(4) and Ti−N(2) bonds (general background 0.21 e Å^{-3}). For complex **11** two residual peaks of 1.54 and 1.24 e Å^{-3} were found near the metal atom along the V−O(1) and V−N(2) bonds (general background 0.35 e Å^{-3}).

Refinements of complexes **5** and **6** were straightforward. In complex **8** the C(23)−C(26) carbon atoms of two ethyl groups showed high thermal parameters, indicating the presence of disorder. The atoms were then split over two positions, called A and B, isotropically refined with site occupation factors of 0.6 and 0.4, respectively, imposing a constraint of 1.54(1) Å to the C−C bond distances. Moreover, the C(41)−C(44) carbon atoms of the thf molecule were found to be distributed over two positions (A and B) isotropically refined with site occupation factors of 0.5. In complex **9** the C(7) and C(8) atoms of one pyrrole ring and some *meso* ethylic chains showed high thermal parameters, indicating the presence of disorder. The disordered atoms were then split over two positions isotropically refined with site occupation factors of 0.65 and 0.35 for the A and B positions, respectively, of C(30), C(32), C(34) and 0.5 for the A and B positions of C(7), C(8), C(25), C(26). The C−C bond distances within the disordered ethyl groups were constrained to be 1.54(1) Å. Here, the toluene solvent molecule of crystallization was found to be statistically distributed along a 2-fold axis. The best fit was obtained by considering the aromatic ring distributed over two positions sharing the C(41), C(41)′, C(43) atoms (′ = $-x$, y, 0.5$-z$) and the methyl carbon over four positions. The "partial" atoms were therefore isotropically refined with site occupation factors of 0.5 for C(42), C(44), C(45) and 0.25 for the A and B positions of C(46). The C−C bond distances within the aromatic ring were constrained to be 1.39(1) Å. During the refinement of complex **11** some significant peaks of height ranging from 1.3 to 2.7 e^{-3} close to an inversion center appeared in the difference Fourier map. These could be interpreted as a centrosymmetric *n*-hexane solvent molecule of crystallization disordered over two positions. However, their unbalanced thermal parameters resulting from the subsequent refinement and the presence of a further residual peak of about 1.1 e^{-3}, inconsistent with the *n*-hexane molecule, suggested the presence of a statistical distribution between *n*-hexane and thf solvent molecules. The best fit was obtained, allowing the site occupation factors to vary freely, converging to 0.8 for C(52), C(53); 0.7 for C(51); 0.5 for C(54), C(55); and 0.3 for C(56), corresponding to a complex/*n*-hexane/thf stoichiometric ratio of 1/0.35/0.3. The position of the oxygen atom of the thf molecule could not be unambiguously established.

Final atomic coordinates are listed in Tables S2−S6 for non-H atoms and in Tables S7−S11 for hydrogens. Thermal parameters are given in Tables S12−S16, and bond distances and angles in Tables S17−S21. Access information is given on any current masthead page.[21]

Scheme 1

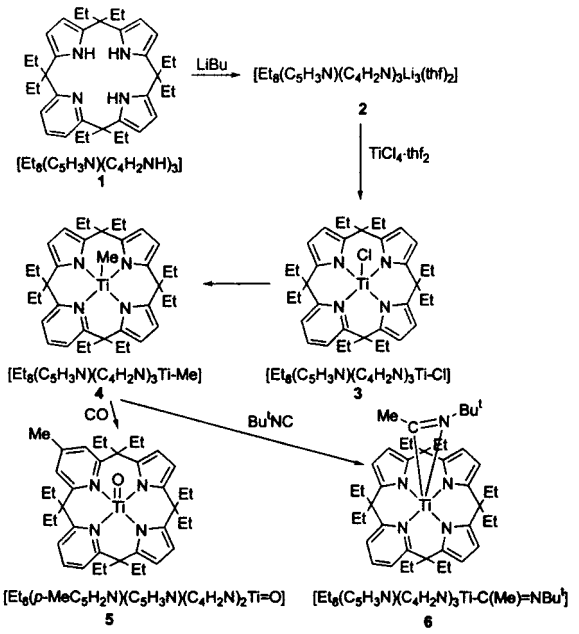

Results and Discussion

Chemical Studies. The synthetic sequence leading to the organometallic functionalization of titanium(IV) bonded to ligand **1** is reported in Scheme 1.

The synthesis and deprotonation of ligand **1** was carried out as previously reported.[6b] The metalation of **2** was carried out in benzene with $TiCl_4$·thf_2, leading to the formation of a violet solid, which was freed from LiCl by extracting it with benzene. The proposed structure for **3**, with all the pyrrolyl anions σ-bonded, is not univocally defined since the ^{1}H NMR spectrum would

(10) Lawton, S. L.; Jacobson, R. A. *TRACER (a cell reduction program)*; Ames Laboratory, Iowa State University of Science and Technology: Ames, IA, 1965.
(11) Lehmann, M.S.; Larsen, F. K. *Acta Crystallogr., Sect. A: Cryst. Phys., Diffr., Theor. Gen. Crystallogr.* **1974**, *A30*, 580−584.
(12) Data reduction, structure solution, and refinement were carried out on a QUANSAN personal computer equipped with an INTEL PENTIUM processor.
(13) Wilson, A. J. C. *Nature* **1942**, *150*, 151.
(14) Ugozzoli, F. *Comput. Chem.* **1987**, *11*, 109.
(15) North, A. C. T.; Phillips, D. C.; Mathews, F. S. *Acta Crystallogr., Sect. A: Cryst. Phys., Diffr., Theor. Gen. Crystallogr.* **1968**, *A24*, 351.
(16) (a) *International Tables for X-ray Crystallography*; Kynoch Press: Birmingham, England, 1974; Vol. IV, p 99. (b) *Ibid.*, p 149.
(17) Stewart, R. F.; Davidson, E. R.; Simpson, W. T. *J. Chem. Phys.* **1965**, *42*, 3175.
(18) Sheldrick, G. M. *SHELX76. Program for crystal structure determination*; University of Cambridge, England, 1976.
(19) Sheldrick, G. M. *SHELX86. Program for the solution of crystal structures*; University of Göttingen, Germany, 1986.
(20) Sheldrick, G. M. *SHELXL92. Program for Crystal Structure Refinement*; University of Göttingen, Göttingen, Germany, 1992.

(21) See paragraph at the end of paper regarding Supporting Information.

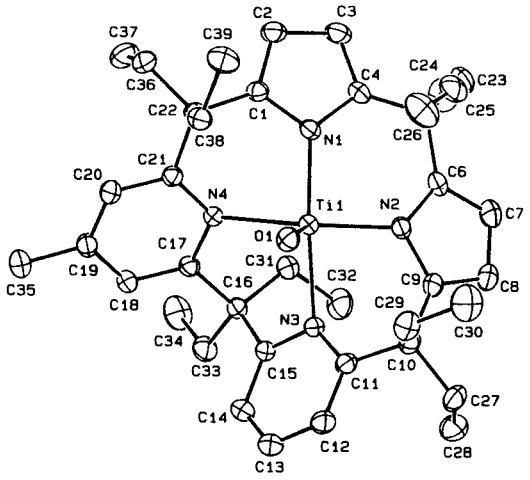

Figure 1. ORTEP drawing of complex **5** (50% probability ellipsoids).

be the same for the $\eta^1:\eta^5:\eta^1$-bonded tris(pyrrole) unit. The alkylation of **3** was carried out in frozen benzene, to avoid reduction of titanium(IV) to titanium(III). This methodology made it possible in several cases to prevent reduction by lithium alkyls leading preferentially to the alkylated products. The methyl derivative **4** underwent a slow but quite clean reaction with carbon monoxide (1 atm) at room temperature. The reaction produced orange crystals of **5** after 4−5 days.

The overall reaction proceeds with the homologation of the pyrrole adjacent to the pyridine ring and with the formation of a *p*-methylpyridine. The regiochemistry producing a *cis*-dipyridine macrocycle is independent of the metal, while the substitution at the pyridine depends on the nature of the metal. Zirconium and hafnium led exclusively to *meta*-substituted,[6] while titanium and niobium to *para*-substituted pyridines.[7c,8a] The occurrence of the homologation reaction[22] has some prerequisites. The first one is the formation of a η^2-acyl having carbenium ion properties.[23,24] Although those are probably not usually as pronounced as in zirconium and hafnium, it seems that they are appropriate in the present case for an intramolecular reaction. The attack of the acyl carbenium ion on the pyrrolyl anion is followed by the complete cleavage of the C−O bond, with the formation of a terminal oxotitanium(IV) derivative, **5**. The regiochemistry of the homologation reaction is discussed in detail in the following section. A Schakal view of **5** is shown in Figure 1. Selected bond distances and angles for complexes **5** and **6** are listed in Tables 2 and 3, respectively; those for complexes **3**, **4**, and **5** are listed in Table 4. Table 5 compares the most relevant conformational parameters of the four complexes. The pyrrole and pyridine rings containing N(1), N(2), N(3), and N(4) are referred to as A, B, C, and D, respectively. The macrocyclic ligand exhibits a $\eta^1:\eta^1:\eta^1:\eta^1$ bonding mode involving two nitrogen atoms from pyrrole rings and two nitrogen atoms from pyridine rings. The coordination polyhedron around titanium is square

Table 2. Selected Bond Distances (Å) and Angles (deg) for Complex 5

Ti(1)−O(1)	1.627(2)	N(2)−C(6)	1.389(4)
Ti(1)−N(1)	2.032(3)	N(2)−C(9)	1.396(3)
Ti(1)−N(2)	2.018(2)	N(3)−C(11)	1.354(3)
Ti(1)−N(3)	2.248(3)	N(3)−C(15)	1.344(3)
Ti(1)−N(4)	2.241(2)	N(4)−C(17)	1.360(4)
N(1)−C(1)	1.390(2)	N(4)−C(21)	1.367(2)
N(1)−C(4)	1.388(4)		
N(3)−Ti(1)−N(4)	90.9(1)	Ti(1)−N(2)−C(9)	121.8(2)
N(2)−Ti(1)−N(4)	154.9(1)	Ti(1)−N(2)−C(6)	124.4(2)
N(2)−Ti(1)−N(3)	84.8(1)	C(6)−N(2)−C(9)	107.0(2)
N(1)−Ti(1)−N(4)	83.7(1)	Ti(1)−N(3)−C(15)	117.0(2)
N(1)−Ti(1)−N(3)	156.5(1)	Ti(1)−N(3)−C(11)	114.4(2)
N(1)−Ti(1)−N(2)	90.6(1)	C(11)−N(3)−C(15)	120.0(2)
Ti(1)−N(1)−C(4)	128.0(2)	Ti(1)−N(4)−C(21)	116.2(2)
Ti(1)−N(1)−C(1)	124.1(2)	Ti(1)−N(4)−C(17)	119.1(2)
C(1)−N(1)−C(4)	107.1(2)	C(17)−N(4)−C(21)	118.3(2)

Table 3. Selected Bond Distances (Å) and Angles (deg) for Complex 6

	molecule A	molecule B
Ti(1)−N(1)	2.015(6)	2.010(5)
Ti(1)−N(2)	2.045(7)	2.053(6)
Ti(1)−N(3)	2.336(5)	2.333(5)
Ti(1)−N(4)	2.000(7)	2.012(4)
Ti(1)−N(5)	2.046(5)	2.052(4)
Ti(1)−C(38)	2.001(6)	2.017(7)
N(1)−C(1)	1.381(11)	1.384(9)
N(1)−C(4)	1.405(9)	1.421(6)
N(2)−C(6)	1.383(8)	1.386(7)
N(2)−C(9)	1.382(10)	1.370(10)
N(3)−C(11)	1.361(10)	1.348(10)
N(3)−C(15)	1.356(8)	1.346(8)
N(4)−C(17)	1.397(8)	1.393(7)
N(4)−C(20)	1.399(10)	1.399(8)
N(5)−C(38)	1.247(10)	1.258(9)
N(5)−C(40)	1.513(10)	1.504(8)
C(38)−C(39)	1.492(11)	1.478(13)
N(5)−Ti(1)−C(38)	35.9(2)	36.0(2)
N(3)−Ti(1)−N(4)	82.2(2)	81.6(2)
N(2)−Ti(1)−N(4)	144.9(2)	144.8(2)
N(2)−Ti(1)−N(3)	88.9(2)	89.2(2)
N(1)−Ti(1)−N(4)	91.2(2)	90.7(2)
N(1)−Ti(1)−N(3)	154.3(2)	152.4(2)
N(1)−Ti(1)−N(2)	82.4(2)	82.0(2)
Ti(1)−N(1)−C(4)	122.8(5)	123.2(4)
Ti(1)−N(1)−C(1)	126.1(5)	127.1(4)
C(1)−N(1)−C(4)	107.1(6)	105.6(5)
Ti(1)−N(2)−C(9)	125.6(4)	125.8(4)
Ti(1)−N(2)−C(6)	121.9(5)	123.2(5)
C(6)−N(2)−C(9)	106.4(6)	107.5(5)
Ti(1)−N(3)−C(15)	114.7(5)	117.0(5)
Ti(1)−N(3)−C(11)	119.8(4)	118.7(4)
C(11)−N(3)−C(15)	119.3(6)	118.8(5)
Ti(1)−N(4)−C(20)	125.9(4)	126.1(4)
Ti(1)−N(4)−C(17)	125.7(5)	125.6(4)
C(17)−N(4)−C(20)	105.6(6)	105.6(4)
Ti(1)−N(5)−C(40)	157.0(5)	156.0(5)
Ti(1)−N(5)−C(38)	70.1(4)	70.5(3)
C(38)−N(5)−C(40)	132.8(6)	133.2(6)
Ti(1)−C(38)−N(5)	74.1(4)	73.5(4)
N(5)−C(38)−C(39)	135.8(7)	135.1(6)
Ti(1)−C(38)−C(39)	149.9(6)	151.4(5)

(22) For a general review on the homologation reaction of alcohols and related species, see: Chiusoli, G. P.; Salerno, G.; Foa, M. In *Reactions of Coordinated Ligands*; Braterman, P. S., Ed.; Plenum: New York, 1986; Vol. 1, Chapter 7. Parshall, G. W.; Ittel, S. D. *Homogeneous Catalysis*, 2nd ed.; Wiley: New York, 1992. Colquhoun, H. M.; Thompson, D. J.; Twigg, M. V. *Carbonylation*; Plenum: New York, 1991.

(23) Durfee, L. D.; Rothwell, I. P. *Chem. Rev.* **1988**, *88*, 1059.

(24) Tatsumi, K.; Nakamura, A.; Hofmann, P.; Stauffert, P.; Hoffmann, R. *J. Am. Chem. Soc.* **1985**, *107*, 4440. Martin, B. D.; Matchett, S. A.; Norton, J. R.; Anderson, O. P. *J. Am. Chem. Soc.* **1985**, *107*, 7952. Roddick, D. M.; Bercaw, J. E. *Chem. Ber.* **1989**, *122*, 1579. Hofmann, P.; Stauffert, P.; Frede, M.; Tatsumi, K.; *Chem. Ber.* **1989**, *122*, 1559. Hofmann, P.; Stauffert, P.; Tatsumi, K.; Nakamura, A.; Hoffmann, R. *Organometallics* **1985**, *4*, 404. Tatsumi, K.; Nakamura, A.; Hofmann, P.; Hoffmann, R.; Moloy, K. G.; Marks, T. J. *J. Am. Chem. Soc.* **1986**, *108*, 4467. Fanwick, P. E.; Kobriger, L. M.; McMullen, A. K.; Rothwell, I. P. *J. Am. Chem. Soc.* **1986**, *108*, 8095. Arnold, J.; Tilley, T. D.; Rheingold, A. L. *J. Am. Chem. Soc.* **1986**, *108*, 5355.

Table 4. Selected Bond Distances (Å) and Angles (deg) for Complexes 8, 9, and 11[a]

	8	9	11
M−N(1)	2.089(7)	1.948(4)	1.986(5)
M−N(2)	1.964(9)	1.960(5)	2.024(4)
M−N(3)	2.221(7)	2.195(4)	2.196(5)
M−N(4)	2.149(10)	2.207(4)	2.178(4)
M−X		2.232(2)	1.829(4)
N(1)−C(1)	1.378(5)	1.389(7)	1.369(6)
N(1)−C(4)	1.400(8)	1.410(7)	1.385(7)
N(2)−C(6)	1.380(8)	1.383(8)	1.361(7)
N(2)−C(9)	1.375(5)	1.379(10)	1.381(6)
N(3)−C(11)	1.348(5)	1.360(8)	1.355(7)
N(3)−C(15)	1.348(5)	1.339(8)	1.379(6)
N(4)−C(17)	1.349(6)	1.354(8)	1.355(6)
N(4)−C(21)	1.354(5)	1.363(8)	1.339(7)
N(3)−M−N(4)	92.6(3)	91.5(2)	83.2(2)
N(2)−M−N(4)	165.8(4)	162.1(2)	156.5(2)
N(2)−M−N(3)	88.7(4)	85.4(2)	82.4(2)
N(1)−M−N(4)	91.2(3)	83.9(2)	96.8(2)
N(1)−M−N(3)	170.3(4)	155.5(2)	146.1(2)
N(1)−M−N(2)	85.5(3)	91.7(2)	85.1(2)
M−O(1)−C(40)			116.9(3)
M−N(1)−C(4)	97.4(3)	125.7(4)	120.7(4)
M−N(1)−C(1)	105.7(4)	124.1(4)	112.1(4)
C(1)−N(1)−C(4)	105.6(4)	106.0(4)	108.4(4)
M−N(2)−C(9)	127.2(4)	124.3(4)	121.1(3)
M−N(2)−C(6)	123.6(4)	127.6(4)	129.0(4)
C(6)−N(2)−C(9)	107.3(4)	107.8(5)	107.6(4)
M−N(3)−C(15)	114.3(3)	120.6(4)	122.0(4)
M−N(3)−C(11)	121.4(4)	118.1(4)	117.6(3)
C(11)−N(3)−C(15)	120.2(4)	119.0(5)	120.0(5)
M−N(4)−C(21)	116.7(4)	116.1(4)	111.5(3)
M−N(4)−C(17)	104.4(3)	114.1(4)	126.1(4)
C(17)−N(4)−C(21)	121.5(4)	120.7(5)	122.0(4)

[a] M should be read Li(1) in **8** and V(1) in **9** and **11**; X should be read Cl(1) in **9** and O(1) in **11**.

pyramidal with the nitrogen atoms at the base and the O(1) oxo oxygen atom at the apex. The metal is displaced by 0.448(1) Å toward the oxygen atom from the N_4 core, which is almost planar, the deviations from planarity ranging from −0.015(2) to 0.015(2) Å. The Ti−O vector forms a dihedral angle of 7.5(1)° with the normal to the N_4 core. The Ti−N bond distances are in good agreement with those observed in the complex [{η^1-η^1-η^1-η^1-Et_8-$(C_4H_2N)_3$(4-MeC_5H_2N)}Ti=O···Li$(Py)_3$],[8a] the Ti−N(pyridine) distances (mean value 2.243(3) Å) being much longer than the Ti−N(pyrrole) distances (mean value 2.022(6) Å), as expected. The Ti−O bond distance (1.627(2) Å) is in the range given by the few reports of oxotitanium species.[25] The macrocycle shows a flattened saddle shape conformation (Table 5), with the A and B pyrrole rings tilted up and the C and D pyridine rings tilted down with respect to the N_4 core. This conformation leads two hydrogen atoms [H(291), H(381)] from two opposite methylene carbons [C(29), C(38)] to approach the oxo oxygen atom. The geometry of these interactions (O(1)···H(291), 2.36 Å; O(1)···C(29), 3.237(3) Å; O(1)···H(291)−C(29), 149°; O(1)···H(381), 2.32 Å; O(1)···C(38), 3.185(4) Å; O(1)···H(381)−C(38), 156°) is consistent with the presence of weak hydrogen bonds.[26] In addition one hydrogen atom [H(311)] from the C(31) methylene carbon is oriented to point toward the sixth site around titanium: Ti···H(311), 2.37 Å; O(1)−Ti···H(311), 156°.

In all the migratory insertions of CO so far carried out on metallaporphyrinogen complexes, we were unable to isolate any η^2-acyl preceding the homologation reaction. However, the isolation of the analogous η^2-iminoacyl **6** was successful due to its much lower reactivity than carbenium ion.[27] The reaction of **3** with Bu^tNC was carried out in benzene and led to dark green crystals of **6**. The rather high C=N (1655 cm^{-1}) stretching vibration is in agreement with a weak carbenium ion centered at the η^1-iminoacyl functionality. The structure of **6** is displayed in Figure 2. In the crystal structure there are two independent complex molecules (called A and B) showing a very close geometry. Data concerning molecule B will be hereafter given in square brackets.

Coordination around titanium is provided by the four η^1:η^1:η^1:η^1-bonded nitrogen atoms from the tris(pyrrole)−mono(pyridine) fragment and by the η^2-N,C-bonded iminoacyl. The metal is displaced by 0.543(2) [0.565(2)] Å from the N_4 core, which shows small but significant tetrahedral distortion, the deviations from planarity ranging from −0.065(6) [-0.050(5)] to 0.078(6) [0.053(5)] Å. The plane of the (η^2-iminoacyl)titanium fragment is perpendicular to the N_4 core (dihedral angle 88.1(3) [88.1(2)]°). The Ti−N(pyrrole) bond distances are different, the Ti−N(1) and Ti−N(4) bond distances (mean value 2.009(7) [2.011(10)] Å) being significantly shorter than Ti−N(2) (2.045(7) [2.053(6)] Å), as a possible consequence of the distortions induced on the macrocycle by the bulky Bu^tNC ligand. The Ti−N(pyridine) bond distance (2.336(5) [2.333(5)]Å) is slightly but significantly longer than those observed in complex **5**. The iminoacyl group is asymmetrically bonded to the metal, the Ti−C(38) bond distance (2.001(6) [2.017(7)] Å) being significantly shorter than the Ti−N(5) bond distance (2.046(5) [2.052(4)] Å). The macrocycle assumes an irregular saddle shape conformation (Table 5), leading the H(261) hydrogen atoms from the C(26) methylene carbon atom to point toward the sixth site around titanium: Ti···H(261), 2.79 [2.76] Å; $C_{N,C}$−Ti···H(261), 157 [158]° ($C_{N,C}$ indicates the center of gravity of the N(5)−C(38) η^2-bonded iminoacyl group).

(25) (a) Yang, C.-H.; Goedken, V. L. *Inorg. Chim. Acta* **1986**, *117*, L19. (b) Yang, C.-H.; Ladd, J. A.; Goedken, V. L. *J. Coord. Chem.* **1988**, *19*, 235. (c) Guilard, R.; Lecomte, C. *Coord. Chem. Rev.* **1985**, *65*, 87. (d) Jeske, P.; Haselhorst, G.; Weyhermueller, T.; Wieghardt, K.; Nuber, B. *Inorg. Chem.* **1994**, *33*, 2462. (e) Comba, P.; Merbach, A. *Inorg. Chem.* **1987**, *26*, 1315. (f) De Angelis, S.; Solari, E.; Floriani, C.; Chiesi-Villa, A.; Rizzoli, C. *Organometallics* **1995**, *14*, 4505. (g) Guilard, R.; Latour, J. M.; Lecomte, C.; Marchon, J. C.; Protas, J.; Ripoll, D. *Inorg. Chem.* **1978**, *17*, 1228. (h) Peng-Ju, L.; Sheng-Hua, H.; Kun-Yao, H.; Ru-Ji, W.; Mak, T. C. W. *Inorg. Chim. Acta* **1990**, *175*, 105. (i) Smith, M. R., III; Matsunaga, P. T.; Andersen, R. A. *J. Am. Chem. Soc.* **1993**, *115*, 7049. (j) Dwyer, N. P.; Puppe, L.; Buchler, J. W.; Scheidt, W. R. *Inorg. Chem.* **1975**, *14*, 1782. (k) Housmekerides, C. E.; Ramage, D. L.; Kretz, C. M.; Shontz, J. T.; Pilato, R. S.; Geoffroy, G. L.; Rheingold, A. L.; Haggerty, B. S. *Inorg. Chem.* **1992**, *31*, 4453. Jeske, P.; Haselhorst, G.; Weyhermüller, T.; Wieghardt, K.; Nuber, B. *Inorg. Chem.* **1994**, *33*, 2462. Smith, M. R.; Matsunaga, P. T.; Andersen, R. A. *J. Am. Chem. Soc.* **1993**, *115*, 7049, and references therein. Gallo, E.; Solari, E.; Franceschi, F.; Floriani, C.; Chiesi-Villa, A.; Rizzoli, C. *Inorg. Chem.* **1995**, *34*, 2495, and references therein.

(26) Hamilton, W. C.; Ibers, J. A. *Hydrogen Bonding in Solids*; Benjamin: New York, 1968.

(27) Iminoacyl formed from migratory insertion of RNC with M−C bonds is a well-known reaction: Singleton, E.; Ossthnizen, H. E. *Adv. Organomet. Chem.* **1983**, *22*, 209. Otsuka, S.; Nakamura, A.; Yoshida, T.; Naruto, M.; Ataba, K. *J. Am. Chem. Soc.* **1973**, *95*, 3180. Yamamoto, Y.; Yamazaki, H. *Inorg. Chem.* **1974**, *13*, 438. Aoki, K.; Yamamoto, Y. *Inorg. Chem.* **1976**, *15*, 48. Bellachioma, G.; Cardaci, G.; Zanazzi, P. *Inorg. Chem.* **1987**, *26*, 84. Maitlis, P. M.; Espinet, P.; Russell, M. J. H. In *Comprehensive Organometallic Chemistry*; Wilkinson, G., Stone, F. G. A., Abel, E. W., Eds.; Pergamon: London, 1982; Vol. 8, Chapter 38.4. Crociani, B. In *Reactions of Coordinated Ligands*; Braterman, P. S., Ed.; Plenum: New York, 1986; Chapter 9.

Table 5. Comparison of Relevant Structural Parameters within the M-Porphyrinogen Units for Complexes 5, 6, 8, 9, and 11

		5	6[a]	8	9	11
distance of atoms from the N_4 core, Å	N(1)	0.015(2)	0.078(6) [0.053(5)]	0.060(4)	−0.046(4)	−0.098(4)
	N(2)	−0.015(2)	−0.065(6) [-0.049(5)]	-0.062(4)	0.099(6)	0.110(4)
	N(3)	0.013(2)	0.046(5) [0.046(5)]	0.031(3)	−0.041(4)	−0.103(4)
	N(4)	−0.013(2)	−0.065(6) [-0.050(5)]	-0.030(3)	0.041(4)	0.092(4)
	M[b]	0.448(1)	0.543(2) [0.565(2)]	0.204(8)	0.394(1)	0.496(2)
distance of M from A,[c] Å		0.296(1)	0.550(2) [0.628(2)]	1.952(7)	0.642(1)	1.332(2)
distance of M from B,[c] Å		0.823(1)	0.809(1) [0.628(1)]	0.384(7)	0.066(1)	0.468(2)
distance of M from C,[c] Å		1.377(1)	1.214(2) [1.230(2)]	0.821(8)	0.770(1)	0.473(2)
distance of M from D,[c] Å		1.229(1)	0.595(2) [0.581(2)]	1.569(8)	1.434(1)	0.218(3)
dihedral angles between the N_4 core and the A, B, C, D rings, deg	(A)	150.1(1)	160.4(2) [160.7(2)]	109.2(2)	142.6(2)	115.4(2)
	(B)	137.4(1)	153.3(2) [153.3(2)]	146.9(1)	155.9(2)	138.4(2)
	(C)	141.6(1)	146.2(2) [146.2(2)]	142.8(1)	146.5(2)	138.5(2)
	(D)	143.9(1)	139.1(2) [139.4(2)]	124.9(1)	139.5(2)	125.7(2)
dihedral angle between AB, deg		160.0(1)	154.5(3) [151.4(3)]	141.6(2)	166.4(3)	155.6(2)
dihedral angle between AD, deg		131.3(1)	151.7(3) [151.1(3)]	100.9(1)	122.4(3)	111.4(2)
dihedral angle between BC, deg		117.3(1)	122.8(2) [125.6(2)]	117.1(2)	137.4(3)	106.1(2)
dihedral angle between CD, deg		105.7(1)	119.9(3) [119.8(3)]	97.5(1)	107.5(2)	123.9(2)

[a] Values in square brackets refer to molecule B. [b] M should be read Ti(1) in **5** and **6**; Li(1) in **8**; V(1) in **9** and **11**. [c] A, B, C, and D define the pyrrole and pyridine rings containing the N(1), N(2), N(3), and N(4) nitrogen atoms, respectively.

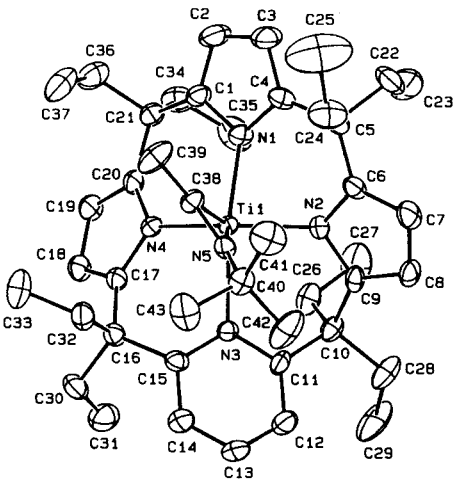

Figure 2. ORTEP drawing of complex **6** (50% probability ellipsoids).

To improve our understanding of the homologation reaction and its limit, we used the bis(pyridine)−bis(pyrrole) macrocycle with a monofunctionalizable metal, i.e., vanadium(III). Such an approach is summarized in Scheme 2. The synthesis of ligand **7** was carried out as reported in the Experimental Section[6b] using the assistance of zirconium rather than titanium(IV). Ligand **7** was deprotonated to **8**, which is then a suitable form for metalation.

The structure of **8** is shown in Figure 3. The Li(1) cation is η^1:η^1:η^1:η^1-bonded to the four nitrogen atoms of the N_4 core. The Li(2) cation is η^1-bonded to the A pyrrole ring through the N(1) nitrogen atom and η^2-bonded to the B pyrrole ring through the N(2), C(6) atoms (Li(2)−N(2), 2.053(10) Å; Li(2)−C(6), 2.433(12) Å). The separations between Li(2) and the other carbon atoms of the B pyrrole ring (ranging from 2.932(9) to 3.633(11) Å) rule out any possible Li(2)−C interaction. Coordination around Li(2) is completed by the oxygen atom from a thf molecule. The Li(1) cation is displaced by 0.204(8) Å from the N_4 core, which shows significant tetrahedral distortions ranging from −0.062(4) to 0.060(6) Å. The Li−N bond distances involving the anionic N(1) and N(2) nitrogen atoms range from 1.951(8) to 2.089(7) Å.[5a] The Li(1)−N(pyridine) bond distances are

Scheme 2

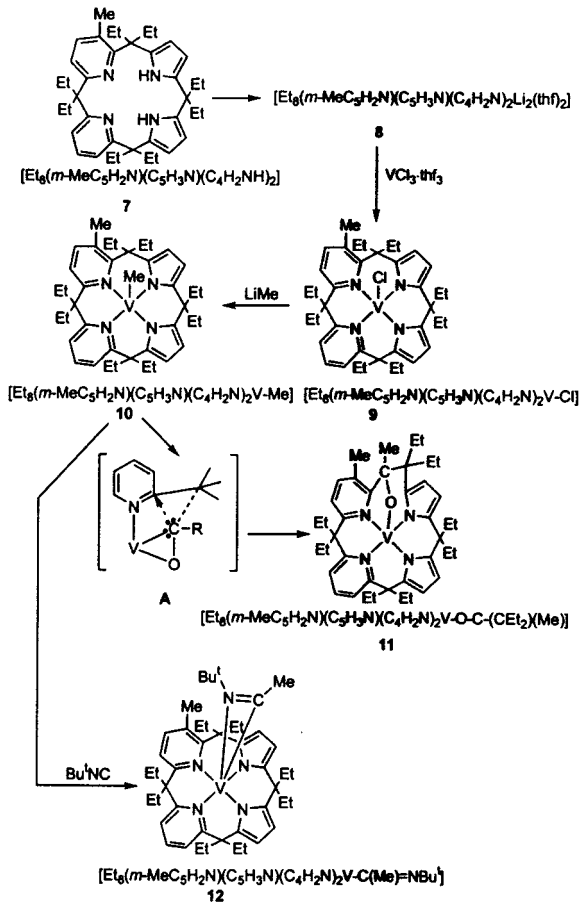

in the range expected for neutral nitrogens binding lithium cations.[28] The macrocycle assumes an irregular conformation with A, B, and C rings tilted up and the D ring tilted down with respect to the N_4 core. This conformation brings the A ring nearly perpendicular to the N_4 core (dihedral angle 109.2°) and the C and D pyridine rings nearly perpendicular to each other (dihedral angle 97.5(1)°).

The reaction of **8** with VCl_3·thf_3 produced yellow crystals of **9**, which is the appropriate starting material

(28) Mulvey, R. E. *Chem. Soc. Rev.* **1998**, *27*, 339.

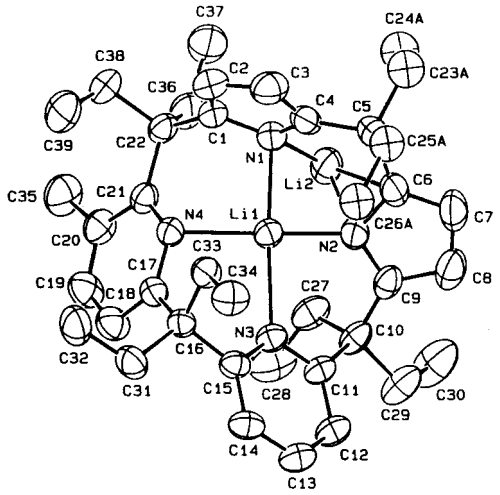

Figure 3. ORTEP drawing of complex **8** (50% probability ellipsoids). The THF molecule bonded to Li(2) and the B positions of the disordered atoms have been omitted for clarity.

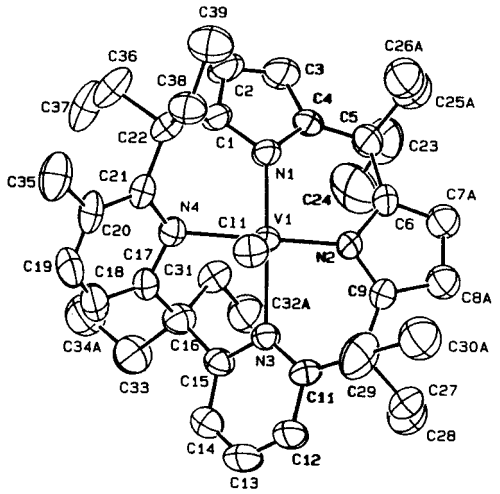

Figure 4. ORTEP drawing of complex **9** (50% probability ellipsoids). Disorder has been omitted for clarity.

for the organometallic functionalization. Complex **9** was fully characterized, including an X-ray analysis, and a picture of its structure is shown in Figure 4. Vanadium exhibits a square pyramidal coordination with the four nitrogen atoms from the ligand at the base and a chlorine atom at the apex. The metal is displaced by 0.394(1) Å from the N_4 core, which shows significant tetrahedral distortions from planarity, the displacements from the mean plane ranging from −0.046(4) to 0.099(6) Å. The V−Cl vector forms a dihedral angle of 12.4(1)° with the normal to the mean plane through the N_4 core. The complex shows an irregular shape due to the twisting of the pyridine ring containing N(4), which is tilted up with respect to the N_4 plane, while the other three rings are tilted down. The conformation of the macrocycle leads two opposite methylene carbons to approach the chlorine ligand at close contacts of 3.416(11) Å for C(29)···Cl(1) and 3.474(7) Å for C(38)···Cl(1). A close intramolecular contact involves the vanadium atom and the H(311) hydrogen atom from the C(31) methylene carbon.

Complex **9** undergoes alkylation reactions illustrated by the formation of **10** in the case of LiMe. The structure we propose for **10** is by analogy the same as that

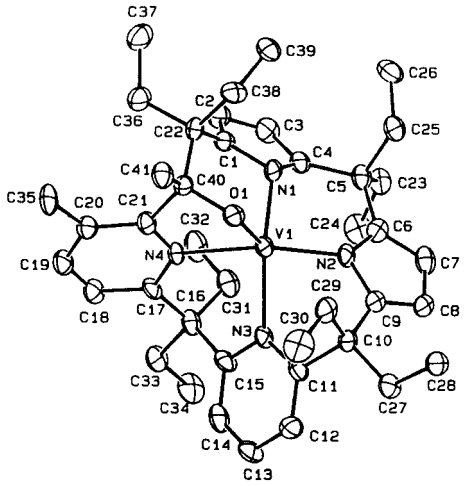

Figure 5. ORTEP drawing of complex **11** (30% probability ellipsoids).

determined for **9**. The conventional analytical data, including the $\mu_{eff} = 2.85\ \mu_B$ at 300 K, are in agreement with the proposed formula. The presence of a V−Me functionality in **10** has been inferred from the results of its reaction with carbon monoxide. The reaction proceeds, very probably, via the intermediate formation of a η^2-acyl. In the case of vanadium, however, the nucleophilic nature of the acyl-carbenoid (see next section) favors the attack to the α-position of the pyridine instead of the pyrrole ring, as in the case of titanium. The overall result is the insertion of the acyl between the pyridine α-position and the *meso*-carbon. An additional factor that does not favor the attack to the pyrrolyl anions is the exclusive η^1-bonding mode to vanadium, as we found in the porphyrinogen−vanadium complexes.[29]

In the case of **11**, the attack by the acyl functionality to the pyridine ring is not accompanied, as in the homologation reaction, by the cleavage of the C−O bond (see previous section on titanium). There are some significant precedents for the attack by η^2-acyl carbene ion on the pyridine.[30] This reactivity has never been observed in the case of η^2-acyl vanadium(III) derivatives, where the metal has a rather low oxophilicity compared with Zr(IV) or Hf(IV).

The structure of **11** was elucidated by an X-ray analysis, and its structure is depicted in Figure 5. The bonding mode of the macrocyle is the same as that observed in complex **9**, as far as the inner core of nitrogen atoms is concerned. However, as a consequence of the insertion of the η^2-acyl, the macrocyclic ligand turns out to be pentadentate, interacting with vanadium through the O(1) oxygen atom at a V(1)−O(1) [1.829(4) Å] distance consistent with a single bond. The V(1)−O(1) bond results in the formation of two puckered five- and six-membered chelation rings. The vanadium atom lies at 0.496(2) Å from the N_4 core, which shows remarkable tetrahedral distortions ranging from −0.103(4) to 0.110(4) Å. The V−O line forms a dihedral angle of 31.7(2)° with the normal to the N_4 mean plane. Neither the V−N(pyrrole) bond distances (mean value

(29) Solari, E.; Musso, F.; Floriani, C.; Chiesi-Villa, A.; Rizzoli, C. *J. Chem. Soc., Dalton Trans.* **1994**, 2015.
(30) Fanwick, P. E.; Kobriger, L. M.; McMullen, A. K.; Rothwell, I. P. *J. Am. Chem. Soc.* **1986**, *108*, 8095.

2.009(18) Å) nor the V−N(pyridine) bond distances (mean value 2.185(9) Å) are significantly different from those observed in **9**. Two hydrogen atoms from the *meso*-ethyl groups appear to complete the coordination sphere around vanadium: V(1)−H(291), 2.48 Å; V(1)−H(312), 2.47 Å, H(291) being *cis* to the O(1) oxygen atom (O(1)−V(1)−H(291), 69°), H(312) being on the opposite side. The dihedral angles formed by these lines with the normal to the N_4 mean plane are 38.1° and 10.3°, respectively. Although the intermediate η^2-acyl cannot be intercepted in the reaction of **10** with carbon monoxide, the corresponding η^2-iminoacyl **12** has been isolated from the reaction of **10** with Bu^{t}NC. The rather weak carbenium ion properties of the η^2-iminoacyl did not lead to any further change, thus allowing it to be isolated.

Extended Hückel Analysis. Here we report extended Hückel calculations[31] designed to reveal the electronic structure and the reactivity patterns of some of the titanium and vanadium complexes supported by the *meso*-octaethyl mono(pyridine)−tris(pyrrole) and bis(pyridine)−bis(pyrrole) macrocycles. In particular, we considered (i) the homologation of one pyrrole ring to pyridine via the formation of a titanium η^2-acyl having carbenium ion properties and (ii) the attack by a nucleophilic vanadium(III) η^2-acyl to the pyridine ring. We will try to give a rationale for the different behaviors of the two metal-η^2-acyls.

The *meso*-octaethyl mono(pyridine)−tris(pyrrole) and bis(pyridine)−bis(pyrrole) macrocycles have been slightly simplified by replacing them with one pyridine and three pyrrolyl anions or two pyridines and two pyrrolyl anions and symmetrizing to a C_s geometry. This simplified model retains the main features of the whole ligand. In particular, the geometrical constraints on the set of the heterocyclic ring ligands have been maintained by fixing their geometry to the experimental X-ray values.

We first considered the [Ti(IV) mono(pyridine)−tris(pyrrole)] fragment in the experimental X-ray geometry observed for the iminoacyl complex **6**. The energy levels are shown on the left of Figure 6 and are characterized by four low-lying empty metal-based orbitals. The $d_{x^2-y^2}$ (not reported in Figure 6), pointing more closely toward the nitrogen atoms, are pushed higher in energy (more than −7 eV), while the remaining four d orbitals are found within 1 eV. The LUMO is the 2a′(d_{z^2}), with the 3a′(d_{xz}) only 0.2 eV higher and the 3a″(d_{xy}) at 0.5 eV. In the C_s point group, the d_{z^2} and d_{xz} components belong to the same a′ symmetry and are significantly mixed, giving rise to a slight bending of the d_{z^2} orbital toward the pyrrole bisected by the *xz* plane and to an enhancement of the d_{xz} lobe pointing toward pyridine. The 4a″(d_{yz}) orbital pointing toward the two pyrrole nitrogens in the *yz* plane lies ∼0.8 eV higher than the 3a′(d_{xz}) pointing toward one pyrrole and a less coordinating pyridine nitrogen in the *xz* plane. These energy levels dictate the geometry and the reactivity of this fragment.

For a Ti(IV) species with a d^0 electron count the LUMO is the 2a′(d_{z^2}) and allows the interaction with a fifth σ-donor ligand along the *z* axis. This is in agreement with the experimental evidence of the [Ti mono(pyridine)−tris(pyrrole)] fragment to form square pyramidal complexes with σ-donor ligands such as a chlorine or an alkyl group. Figure 6 illustrates the orbital interaction diagram for the methyl complex, taken as an example, and shows the main bonding interaction between the empty 2a′(d_{z^2}) metal orbitals and the occupied σ orbital of Me^-. The remaining three metal orbitals are unaffected by this interaction, which leaves the 3a′(d_{xz}) as the LUMO of the alkyl complex with important consequences on their reactivity pattern (see below).

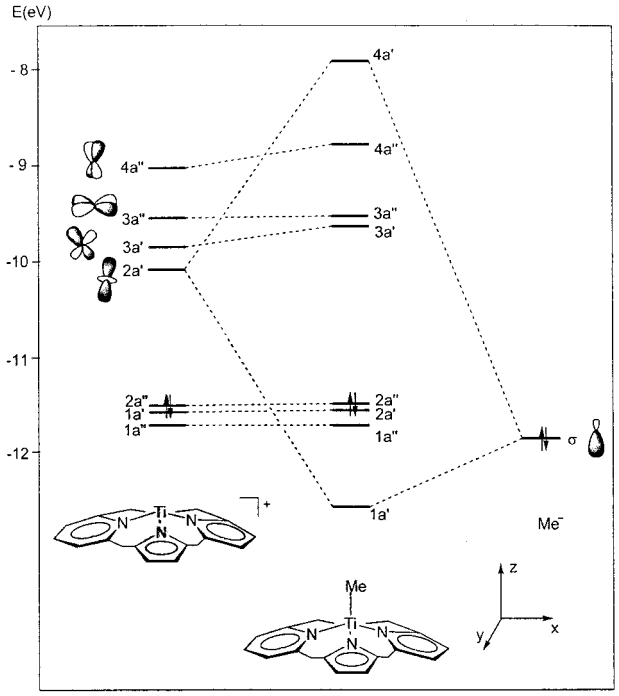

Figure 6. Molecular orbital interaction diagram for [H_8-(C_5H_3N)(C_4H_2N)$_3$Ti−Me].

We then considered the possible reaction pathways following the attack of a nucleophile such as carbon monoxide or isonitriles. Both the high charge calculated on the titanium atom (+1.9) and the metal localization of the LUMO orbital suggest the attack of this nucleophile on the metal atom leading to its insertion into the Ti−R bond. Indeed, the CO or isonitrile insertion into the Zr−R bond is a classic reaction in organometallic chemistry.[23] The reaction proceeds initially to the formation of an η^2-acyl or η^2-iminoacyl species and then, depending on the ligands available on the metal center, to several possible outcomes. In the present case, while an η^2-iminoacyl species has been isolated and structurally characterized, the insertion of carbon monoxide has been observed to lead exclusively to the final expansion of one of the three pyrrole rings of the N_4 ligand to pyridine. Previous calculations[32] have shown that the reactivity of such an η^2-acyl coordinated to a d^0 metal center can be described in terms of a "carbenium-type" character and is determined by the presence of a low-lying LUMO, made up essentially of the π^*_{co} perpendicular to the acyl plane.[32] Such an empty low-lying π^*_{co} makes the acyl carbon strongly electrophilic and there-

(31) Hoffmann, R.; Lipscomb, W. N. *J. Chem. Phys.* **1962**, *36*, 2179. Hoffmann, R. *J. Chem. Phys.* **1963**, *39*, 1397.

(32) Tatsumi, K.; Nakamura, A.; Hofmann, P.; Stauffert, P.; Hoffmann, R. *J. Am. Chem. Soc.* **1985**, *107*, 4440. Tatsumi, K.; Nakamura, A.; Hofmann, P.; Hoffmann, R.; Moloy, K. G.; Marks, T. J. *J. Am. Chem. Soc.* **1986**, *108*, 4467.

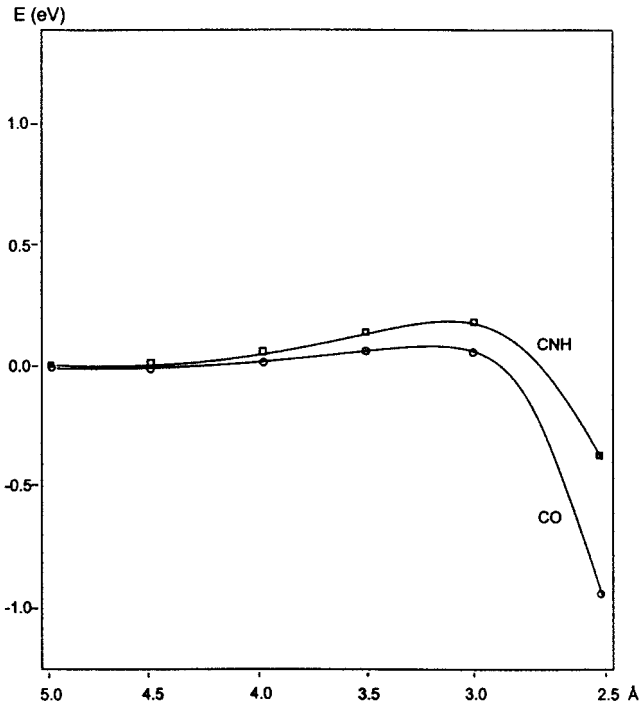

Figure 7. Energy profiles for the attack by CO and HNC to [$H_8(C_5H_3N)(C_4H_2N)_3Ti-Me$].

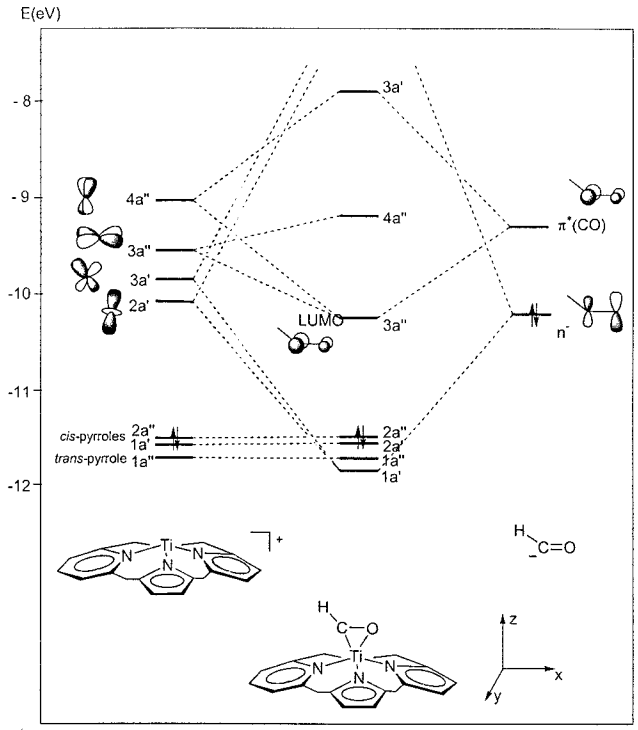

Figure 8. Molecular orbital interaction diagram for [$H_8(C_5H_3N)(C_4H_2N)_3Ti(\eta^2$-CHO)].

fore highly reactive toward electron-rich substrates, such as one of the unsatured pyrrolyl anions.

To confirm that this mechanism operates also in the [Ti mono(pyridine)−tris(pyrrole)] alkyl complexes, we have considered the insertion of carbon monoxide and methyl isonitrile into the Ti−Me bond and the electronic structures of the η^2-acyl and η^2-iminoacyl species. The most favorable approach of the CO and MeNC nucleophiles is determined by the spatial extension of the 3a′-(d_{xz}) LUMO, which suggests the attack occurs in the *xz* plane (the plane where pyridine and pyrroles are coordinated) along a line forming an angle of approximately 45° with the *z* axis on the pyridine side. We simulated the initial stages of the attack by performing extended Hückel calculations on the [Ti mono(pyridine)−tris(pyrrole)−Me]−CO and [Ti mono(pyridine)−tris(pyrrole)−Me]−CNMe systems with different carbon-to-metal distances from 5.0 to 2.5 Å along a line in the *xz* plane, relaxing the axial position of the Me ligand and the angular position of the attacking nuclophile at each point along the attack pathway. The calculated total energy profiles are reported in Figure 7 and show negligible energy barriers (0.1 and 0.2 eV, respectively, at ca. 3 Å) followed by a significant stabilization, thus supporting a facile insertion of both nucleophiles into the Ti−Me bond.

Next, we considered the η^2-coordinated acyl and iminoacyl complexes [Ti mono(pyridine)−tris(pyrrole)-(η^2-MeCO)] and [Ti mono(pyridine)−tris(pyrrole)])(η^2-MeCNH)]. We took for both η^2-coordinated moieties the orientation observed for the structurally characterized η^2-iminoacyl complex **6** with the acyl or iminoacyl plane lying in the *xz* symmetry plane and used the experimental geometry for the iminoacyl species. For the acyl complex we used the same Ti−C and Me−C distances and fixed the Ti−O distance to 1.98 Å, the C−O distance to 1.21 Å, and the MeCO angle to120°. The bonding between the metal fragment and the acyl moiety is illustrated by the interaction orbital diagram in Figure 8. On the extreme right of Figure 8 we show the two highest frontier orbitals of the acyl ligand, i.e., the HOMO n_-, consisting of the out-of-phase combination of the carbon and oxygen p_z orbitals and the LUMO π^*-(CO) orbital. We see that the titanium−acyl bonding is mainly achieved through the interaction between the metal d_{z^2} and d_{xz} orbitals with the acyl n_- orbital.

Note that the LUMO of this hypothetical η^2-acyl complex has an essentially acyl π^*(CO) character and appears at even lower energy than the π^*(CO) orbital of the acyl fragment because of the interaction with the d_{yz} and d_{xy} metal orbitals. This low-lying LUMO, whose larger component is a carbon p_π, makes the η^2-coordinated acyl moiety strongly electrophilic at the carbon atom and gives it a carbene-like character, which has been theoretically investigated[33] and rationalized in terms of a contribution of the oxycarbene resonance hybrid **E** (see Chart 2) to the ground-state properties of the acyl complex. The carbenoid character of the η^2-coordinated acyl ligand is expected to increase with the oxophilicity of the metal, which stabilizes the oxycarbene valence structure **E**.

The nature of the η^2-coordinated acyl moiety suggests two possible mechanistic pathways for the pyrrole ring expansion. If the η^2-acyl behaves as a carbene, it can add to the C_2-C_3 (C_3-C_5) bond of the pyrrole with opening of the initially formed cyclopropyl ring to a *meta*-substituited pyridine, **F** in Chart 2. If, on the other hand, the η^2-acyl behaves as a carbenium ion, it can migrate to the C_2 or C_3 (C_5 or C_4) carbon atoms of the pyrrole, giving an acetylpyrrole η^1-bonded to the tita-

(33) (a) Villiers, C.; Adam, R.; Ephritikhine, M. *J. Chem. Soc., Chem. Commun.* **1992**, 1555. (b) De Boer, E. J. M.; De With, J. *J. Organomet. Chem.* **1987**, *320*, 289. (c) Meyer, T. Y.; Messerle, L. *J. Am. Chem. Soc.* **1990**, *112*, 4564.

Chart 2

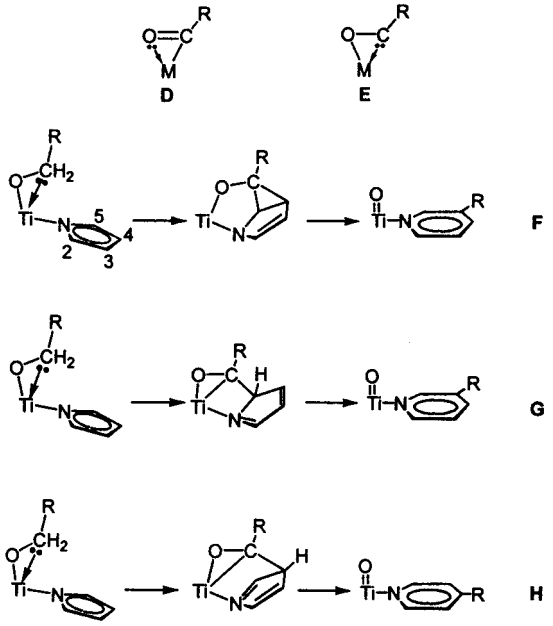

Chart 3

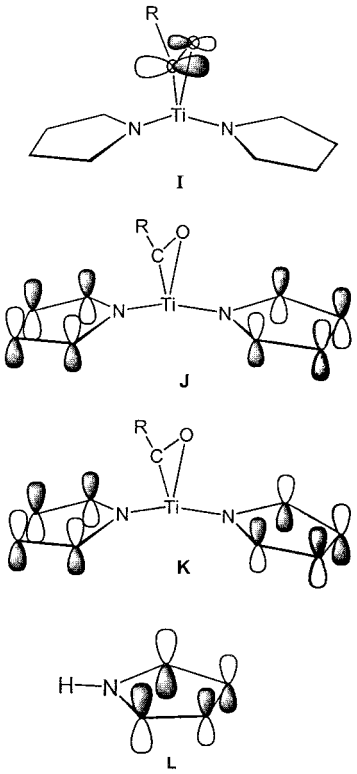

nium, which is then deoxygenated by the metal to give a *meta*-substituited or a *para*-substituited pyridine, respectively, **G** and **H** in Chart 2. In both cases, the main driving force for the overall reaction is the oxophilicy of the titanium, which allows the C−O scission. Analogous mechanisms have been proposed for the ring expansion of pentamethylcyclopentadienyl anion to alkylbenzene in the carbonylation of $[(\eta^5\text{-}C_5Me_5)_3UR)]$[32a] and $[(\eta^5\text{-}C_5Me_5)_2Ti(\eta^2\text{-}COR)]$[32b] and in the reduction of $[(\eta^5\text{-}C_5Me_5)Ta(\eta^2\text{-}COR)Cl_3]$.[32c]

Two major aspects still have to be understood in the regiochemistry of the pyrrole to pyridine ring expansion, which leads exclusively to (i) the homologation of the pyrrole ring *cis* to pyridine and (ii) the expansion of the pyrrole to the *para*-substituted pyridine. The regiochemistry producing a *cis*-bispyridine macrocycle can be easily explained on the basis of the geometric and electronic structure of the η^2-acyl complex. The X-ray structure of the η^2-iminoacyl complex, which is expected to be very close to that of the hypothesized η^2-acyl species, already suggests that the two pyrrole rings adjacent to pyridine have the suitable orientation and the geometrical proximity for a facile attack by the η^2-acyl group. This is further supported by the spatial extension of the low-lying LUMO, responsible of the acyl electrophilic character, which is essentially a π^*(CO), **L** in Chart 3, and is therefore suitably oriented toward the π-system of the adjacent pyrrolyl anion. Moreover, the two highest-lying MOs are mainly constituted by the in-phase and out-of-phase combinations of the π_3^*-like orbitals of the two pyrrolyl anions *cis* to the pyridine ring (**J** and **K** in Chart 3) and are higher than the π_3^*-like orbital of the pyrrolyl anion *trans* to the pyridine, which is stabilized by the stronger interaction with the metal d_{yz} orbitals which, at variance with the d_{xz}, is not involved in the electron donation from the η^2-coordinated acyl ligand. Both factors make the two *cis* pyrrolyl anions more nucleophilic than the *trans* pyrrolyl ring and therefore more susceptible to the acyl attack.

Harder to explain is the regiochemistry of the pyrrole to pyridine ring expansion, which depends on the nature of the metal, leading to *meta*-substituted pyridine for zirconium and hafnium and to *para*-substituted pyridine for titanium and niobium. These different behaviors can be explained on the basis of the effect of the particular metal chosen on (i) the character of the η^2-acyl moiety and (ii) the spatial location of the highest occupied MOs mainly located on the pyrrole rings.

In the present case, the moderate oxophilic character of titanium suggests a low carbene character of the η^2-acyl, which would favor the carbenium ion mechanisms **G** or **H**. The regiochemistry of the electrophilic attack of the η^2-acyl moiety on the pyrrole ring is then determined by charge and frontier orbital factors.[34] The Mulliken analysis of the [Ti mono(pyridine)−tris(pyrrole)(η^2-MeCO)] complex shows that the C_3 atom of the *cis* pyrrole rings bears a negative charge (−0.23), while the corresponding C_2 atom has a slight positive charge (+0.15). At the same time, the two highest occupied MOs responsible for the nucleophilic character of the pyrrole rings are slightly more localized on C_3 and C_4 atoms rather than on C_2 and C_5. Therefore, both charge and frontier orbital arguments favor mechanism **H**, the acyl group migrating preferentially on C_3 or C_4 and then rearranging to the *para*-substituted pyridine in agreement with the experimental evidence. Note that the regiochemistry of the electrophilic attack of the η^2-acyl moiety on the pyrrole ring is different than the usual regiochemistry of the electrophilic substitution on the free pyrrole which is directed to the C_2 position.[35] This difference is due to the effect of the η^1-bonded metal on the π electron distribution on the two *cis* pyrrole rings in the [Ti mono(pyridine)−tris(pyrrole)(η^2-MeCO)] com-

(34) Fleming, I. *Frontier Orbitals and Organic Chemical Reactions*; Wiley: London, U.K., 1976.

(35) Eicher, T.; Hauptmann, S. *The Chemistry of Heterocycles*; George Thieme Verlag: Stuttgart, Germany, 1995.

plex. In particular, while the π_3* HOMO of free pyrrole is preferentially located on the C_2 and C_5 positions, **L** in Chart 3, the two highest occupied MOs of [Ti mono(pyridine)−tris(pyrrole)(η^2-MeCO)] are slightly more localized on C_3 and C_4 atoms of the two *cis* pyrrole rings, **J** and **K** in Chart 3. It is worth noting that the introduction of a bulky or an electron-attracting group on the nitrogen of pyrrole has been employed in organic syntheses to direct the electrophilic attack on pyrrole at the C_3 position.[36]

In the case of zirconium and hafnium, the higher oxophilic character of these metals suggests a higher carbene character of the η^2-acyl moiety and, hence, could favor the carbenium ion mechanism **G**, leading to a *meta*-substituted pyridine. Note that this is the same regiochemistry observed for the cycloaddition of pyrroles with chlorocarbene.[35]

The extended Hückel calculations on the η^2-iminoacyl complex show a bonding interaction between the metal fragment and the iminoacyl moiety quite similar to that discussed above for the η^2-acyl complex. A more detailed comparison of the orbital energies and Mulliken charges of [Ti mono(pyridine)−tris(pyrrole)(η^2-MeCO)] and [Ti mono(pyridine)−tris(pyrrole)(η^2-MeCNH)] helps to explain the different behavior of the [Ti−R] functionality toward the migratory insertion of carbon monoxide or isocyanides. Indeed, once the insertion has taken place, giving rise to the η^2-acyl or to the η^2-iminoacyl intermediate, the reactivity of these latter species toward the migration to a pyrrole ring is determined by the electrophilic character of the acyl or iminoacyl carbon. The higher the electrophilicity of the acyl or iminoacyl carbon, the more favored the migration. The electrophilic character is determined by the availability of the low-lying orbital of π^*_{CO} or π^*_{CN} character (see above) and also by the charge on the acyl or iminoacyl carbon itself. We found a π^*_{CN} orbital in the η^2-iminoacyl species higher than the π^*_{CO} orbital in the η^2-acyl (−9.9 vs −10.3 eV, respectively) and a much lower charge on the iminoacyl carbon than on the acyl one (+0.27 vs +0.59, respectively), both effects indicating clearly a higher electrophilicity of the acyl species. Therefore, while the acyl moiety undergoes a facile migration to an electron-rich pyrrole ring leading to its homologation to pyridine, the lower electrophilicity of the iminoacyl carbon prevents its migration, leading to a stable η^2-iminoacyl complex.

We then considered the [V(III) bis(pyridine)−bis(pyrrole)] fragment in the experimental X-ray geometry observed for the chlorine complex **9**. The energy levels are shown on the left of Figure 9 and are again characterized by four low-lying empty metal-based orbitals. Choosing the reference axes so that *xz* is the symmetry plane bisecting the N(pyrrole)−V−N(pyrrole) and N(pyridine)−V−N(pyridine) angles as shown in Figure 9, it is now the d_{xy} that points toward the nitrogen atoms and is pushed high in energy, while the remaining four d orbitals are found within only 0.4 eV. The LUMO is the 2a′(d_{z^2}) with the 3a′(d_{xz}) only 0.1 eV higher, although the d_{z^2} and d_{xz} components belong to the same a′ symmetry and are strongly mixed. This mixing gives rise to a significant bending of the d_{z^2} orbital toward the pyrroles and to an enhancement of

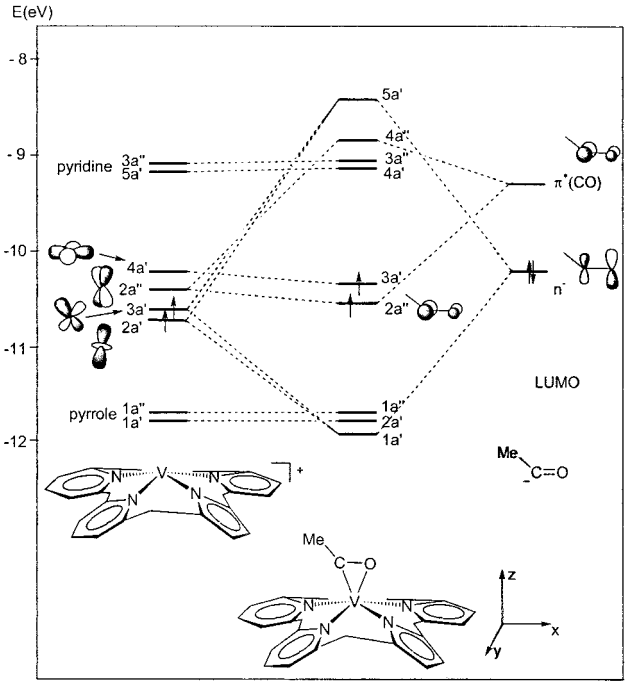

Figure 9. Molecular orbital interaction diagram for [H_8-($C_5H_3N)_2$($C_4H_2N)_2$V(η^2-MeCO)].

the d_{xz} lobe pointing toward the pyridines. Slightly higher in energy are the 2a″(d_{yz}) and 4a′($d_{x^2-y^2}$) orbitals, respectively 0.2 and 0.4 eV above the 2a′. It is worth noting that, despite their remarkable difference, the two *meso*-octaethyl mono(pyridine)−tris(pyrrole) and bis(pyridine)−bis(pyrrole) macrocycles lead to almost isolobal metal fragments and then to similar bonding capabilities. Therefore, the different reaction patterns of the two [Ti mono(pyridine)−tris(pyrrole)] and [V bis(pyridine)-bis(pyrrole)] fragments are essentially due to the different metal configurations, d^0 and d^2, respectively (see below).

Analogously to the monopyridine titanium complex, the lowest metal orbital of the bispyridine vanadium fragment is the 2a′(d_{z^2}), which still allows the interaction with a fifth σ-donor ligand along the *z* axis, in agreement with the experimental evidence of the [V bis(pyridine)−bis(pyrrole)] fragment to coordinate σ-donor ligands such as a chlorine or an alkyl group. The asymmetry of the 2a′(d_{z^2}) orbital suggests a bending of the apical ligand, in agreement with the dihedral angle of 12.4° formed by the V−Cl vector with the normal to the mean plane through the N_4 core in complex **9**. The orbital interaction diagram for the vanadium methyl complex is therefore qualitatively similar to that for the titanium complex in Figure 6, showing as main bonding interaction that between the empty 2a′(d_{z^2}) metal orbitals and the occupied σ orbital of Me^-. The remaining three metal orbitals are unaffected by this interaction and remain very close in energy, giving rise to a high-spin V(III) d^2 species, in agreement with the observed magnetic behavior of **10**.

We next considered the insertion of carbon monoxide and methyl isonitrile into the Ti−Me bond and the electronic structures of the η^2-acyl and η^2-iminoacyl species.

The most favorable approach of the CO and MeNC nucleophiles is determined by the spatial extension of

(36) Anderson, H. J.; Loader, C. E. *Synthesis* **1985**, 353.

the 3a′(d_{xz}) LUMO, which suggests the attack occurs in the *xz* plane along a line forming an angle of approximatively 45° with the *z* axis from the side where the two pyridine are coordinated. We simulated the initial stages of the attack by performing extended Hückel calculations on the [V bis(pyridine)−bis(pyrrole) Me]−CO and [V bis(pyridine)−bis(pyrrole)Me]−CNH systems with different C-to-metal distances, from 5.0 to 2.5 Å, relaxing the axial position of the Me ligand and the angular position of the attacking nuclophile at each point along the attack pathway. The calculated total energy profiles show small energy barriers (0.4 and 0.6 eV, respectively) followed by a significant stabilization, thus supporting a facile insertion of both nucleophiles into the V−Me bond.

We also considered the η^2-coordinated acyl and iminoacyl complexes [V bis(pyridine)−bis(pyrrole)(η^2-MeCO)] and [V bis(pyridine)−bis(pyrrole)])(η^2-MeCNH)]. We took for the metal fragment the X-ray geometry of the methyl complex **10** and for the η^2-coordinated acyl and iminoacyl ligands the same geometries (see above) used for the corresponding titanium species, correcting the V−C, V−O, and V−N distances by the covalent radius difference between Ti(IV) and V(III). The bonding between the metal fragment and the acyl moiety is illustrated by the interaction orbital diagram in Figure 9. As in the titanium complex, the metal−acyl bonding is mainly achieved through the interaction between the metal d_{z^2} and d_{xz} orbitals with the acyl n_- orbital. Figure 9 shows that two unpaired electrons occupy two isolated, almost degererate 3a′ and 2a″ MOs, respectively a metal $d_{x^2-y^2}$ and an orbital of mainly acyl-π*(CO) character, which, as in the titanium case, falls at even lower energy than the π*(CO) orbital of the acyl fragment due to the interaction with the d_{yz}. Note that, at variance with the titanium η^2-acyl, this latter orbital is occupied by one electron and therefore gives to the acyl moiety a nucleophilic character rather than the usual electrophilic character observed in most of the group IV metals or actinides η^2-acyl complexes. This explains the unusual reactivity of this hypothesized acyl intermediate that shows an intramolecular nucleophilic attack at the electron-poor pyridine ring rather than an electrophilic attack at the electron-rich pyrrolyl anion. The regiochemisty of the acyl insertion, exclusively at the *ortho* position of pyridine, is easily explained on the basis of both charge and frontier orbital factors. Indeed, the Mulliken analysis of the [V bis(pyridine)−bis(pyrrole)-(η^2-MeCO)] complex shows that the C_2 and C_6 atoms of the pyridine rings bear the highest positive charge (+0.31), while the C_3 and C_5 or C_4 atoms are almost neutral (+0.08 and −0.05, respectively). At the same time, the two lowest-lying vacant MOs, which are mainly constituted by the in-phase and out-of-phase combinations of the π_4*-like orbitals of the two pyridine and are responsible for their electrophilic character (see Chart 4), are more localized on C_2 and C_6 atoms.

Chart 4

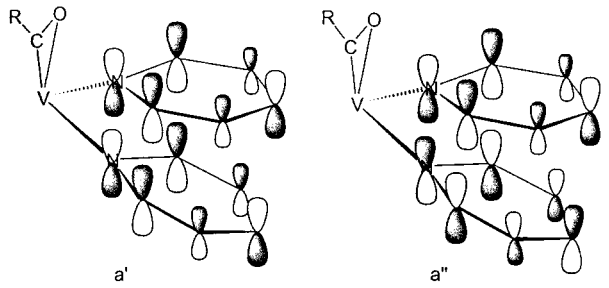

Therefore, both charge and frontier orbital arguments favor an intramolecular nucleophilic attack of the η^2-acyl ligand to the *ortho* position of one of the pyridines followed by its insertion into the C(pyridine)−C(*meso*) bond. In this case, the acyl insertion is not followed, as in the homologation on the titanium complex, by the scission of the C−O bond, probably because of the lower oxophilicity of vanadium. It is worth noting that an analogous mechanism has been proposed for the insertion of η^2-acyls, formed by the CO migratory insertion into the Zr−Me bonds of $Zr(OAr)_2(Me)_2$, into the *ortho* C−H bonds of pyridine.[30]

Conclusions

The migratory insertion reaction of carbon monoxide into Ti−C and V−C bonds in a macrocyclic environment led to some unexpected results. These arise from the enhanced carbenium ion, carbenoid properties of the intermediate η^2-acyl, which is able, in the case of titanium bonded to a mono(pyridine)−tris(pyrrole) macrocycle, to homologate one pyrrole to a pyridine ring and in the meantime to generate a rare terminal oxotitanium(IV) complex. In the case of vanadium bonded to a bis(pyridine)−bis(pyrrole) macrocycle, the reaction of a V−C bond with CO led to the generation of a very reactive η^2-acyl which, as a consequence of the d^2 configuration of the metal, displays a nucleophilic reactivity toward the pyridine ring. The intermediacy of the titanium- and vanadium-η^2-acyl has been proved by the formation of the η^2-iminoacyls under the same conditions in the reaction of Ti−C and V−C bonds with Bu^tNC.

Acknowledgment. We thank the "Fonds National Suisse de la Recherche Scientifique" (Bern, Switzerland, Grant No. 20-53336.98), Ciba Specialty Chemicals (Basle, Switzerland), and Fondation Herbette (University of Lausanne, N.R.) for financial support.

Supporting Information Available: SCHAKAL drawings and X-ray crystallographic files for complexes **5**, **6**, **8**, **9**, and **11**. This material is available free of charge via the internet at http://pubs.acs.org.

OM980888O